VON KARMAN INSTITUTE FOR FLUID DYNAMICS
CHAUSSÉE DE WATERLOO, 72
B - 1640 RHODE SAINT GENÈSE - BELGIUM

STANDARDS FOR PRESSURE MEASUREMENTS IN SUPERSONIC NON-UNIFORM FLOW - AN URGENT NEED

C.H. SIEVERDING & S. SFERRUZZA

TABLE OF CONTENTS

LIST OF SYMBOLS

k	isentropic exponent
L	length of pressure connecting tubes
M	local Mach number
P	pressure
$\Delta\ell$	interference length
ζ	kinetic energy losses

SUBSCRIPTS

o	total
1	upstream
2	downstream
pit	pitot

1. INTRODUCTION

Every person who has been involved in supersonic cascade performance measurements knows how difficult it is to answer questions concerning the accuracy of the measurements and the reliability of the performance data. There are three factors contributing to the uncertainty of the performance data:

(1) measurements errors resulting from:
- inaccurate functioning of parts of the measurement chain (non-linearity of transducers, zero-shift of electronics, etc);
- inaccurate calibration curves;
- inaccurate measurement of probe reference angle;
- fluctuations of overall flow conditions.

(2) measurement errors induced by using probes in non-uniform flow fields albite calibrated in uniform flow only.

(3) non-periodic flow conditions caused by slight variations in blade geometry and, above all, by reflections of shocks and expansion waves from the cascade boundaries back into the outlet flow field.

Of these three contributions, only the first one can be evaluated with some confidence. The order of magnitude of this error in supersonic flow is similar to that in subsonic flow, with the exception that an error in the static pressure affects the loss data to the same degree as an error in the measurement of the total pressure.

Rather little can be done concerning the non-periodic character of the outlet flow field at supersonic outlet Mach numbers. The blade variations of losses, flow angles and static pressure exceed in general by far the uncertainty of these variables due to the first category of measurement errors.

However, the non-periodic character of the outlet flow field related to the finite extension of the cascade, disappears at limit loading conditions.

So far, little attention has been paid to the behaviour of probes in non-uniform supersonic flow fields. Sieverding (Ref. 1) discussed the problem of measuring total and static pressures in different field points with non-identical flow conditions. He also reported an experiment in which a two-finger probe, consisting of a combined total-directional probe head and a separate needle probe for measuring the static pressure, traversed a Prandtl-Meyer expansion. The result is presented in Fig. 1. The occurrence of very high local errors in the PM-expansion field, decided him to abandon the use of needle static pressure probes for supersonic cascade testing.

In view of these few results it appeared interesting to go one step further and investigate the response of a typical combined total-static-directional probe traversing an oblique shock.

2. EXPERIMENTAL SETUP

The tests are carried out in the VKI high speed cascade tunnel C-3. For the present purpose the test section is equipped with a convergent-divergent calibration nozzle. The divergent part of the nozzle has flexible endwalls (Ref. 2), which allows a continuous variation of the nozzle exit Mach number. A 4.5° wedge attached to the lower nozzle wall serves as shock generator (Fig. 2). The tests are conducted at a nozzle exit Mach number of ≈ 1.61. The shock induced by the wedge is rather weak. The Mach number ratio across the shock is $M_2/M_1 \approx 0.90$. The corresponding total ratio is $P_{02}/P_{01}=0.9988$.

The probe is a two-finger probe (Fig. 3). It has a combined total-directional probe head and a separate cone probe for the static pressure. Two different cone probe heads were investigated. The probe heads differ by the position of the sensing holes with respect to the nose tip (1.5 mm for probe A and 2.5 mm for probe B) and the diameter of the sensing holes (0.3 mm for probe A and 0.4 mm for probe B). The bigger hole diameter for probe B implied a bigger distance to the cone tip. Each cone has only 2 holes.

The two static pressure sensing holes and the total pressure sensing hole are ligned up with each other. Due to the oblique cut directional pressure tubes, the directional sensing holes lie slightly downstream of the total pressure hole. The probe traverses the flow field vertically, i.e., normal to the nozzle axis.

Great care was taken to ensure a vibration-free motion of the probe through the shock. The probe motion was controlled visually through the plexiglas side walls.

3. PROBE-SHOCK INTERFERENCE

The Schlieren photographs in Fig. 4 show the probe in various positions with respect to the oblique shock generated by the wedge at the lower nozzle wall. The bow shock generated by the total-directional probe head is clearly visible on all photographs while the weak shock generated by the static cone probe is difficult to detect.

In picture 4a the shock intersects the probe head ≈ 6 mm downstream of the probe tip. The lower part of the probe bow shock interferes with the oblique shock, but the presence of the probe does not seem to alter significantly its structure. In picture 4b the probe tip enters the oblique shock. Now, the shock structure is visibly modified. Contrary to the part below the probe, the upper part appears much more diffuse. However, it is not clear, whether this change is due to the fact that the shock is actually smeared out over a larger distance or whether the interference of the oblique shock with the normal probe shock leads to local unsteady flow conditions. The pressure traces in Fig. 5 seem to support the second explanation (see next paragraph). In picture 4c the shock intersects the cone probe between the pressure holes and the probe tip. The total pressure head has just moved out of the shock and the upper part of the bow wave coincides with the oblique shock. The interference effects appear somewhat weaker than in picture 4b. In the last photograph the probe has moved sufficiently far away from the oblique shock to avoid any interference effects.

Figure 5 shows total pressure traces taken at various fixed positions across the shock wave. These measurements are taken with standard low frequency Statham pressure transducers and rather long connecting lines. Hence, the absence or presence of pressure fluctuations in a given position are therefore only indications for steady or unsteady flow conditions. The probe was displaced in steps of 0.4 mm. Before entering the shock (position A) and as

4. PROBE PRESSURE MEASUREMENTS

4.1. Probe pressure rise through shock

The pressure traces recorded for probe A at two different traversing speeds (0.4 mm/s and 0.8 mm/s) are presented in Fig. 6. In addition to these continuously recorded pressures, stabilized pressure values are shown for a discrete number of probe positions (every 0.4 mm). It is important to note that very short connecting tubes were used. The total distance between probe head and pressure transducer was L=400 mm metal tube of 1 mm inner diameter + 200 mm plastic tube of 4.6 mm inner diameter.

None of the pressure sensing holes records the shock as a discontinuity. The pressure rise through the shock extends from about 1.4 mm for the total pressure to almost 4 mm for the directional probe. Possible causes for the slow pressure rise are:

1. size of pressure sensing holes;
2. interference effects : interference of field shock with probe shocks (in particular with pitot probe bow wave) and with probe boundary layers (in particular on cone head of static pressure probe);
3. response time.

For the stabilized pressure values the length of the pressure rise $\Delta\ell$ depends only on (1) and (2). These values are compared in the table below with the shock interference length due to the hole size only, $\Delta\ell_{geom.}$, see Fig. 7.

	Cause	pitot	static	directional
$\Delta\ell$ (stabilized meas.)	(1)+(2)	1.2	2.0	3.4
$\Delta\ell$ (geometric)	(1)	0.8	0.6	2.2

soon as the probe has moved out of the shock region (position E), the pressure response is absolutely flat. However, as soon as the probe senses the shock, indicated by the beginning pressure rise, pressure fluctuations are observed. These are particularly important in position C. In absence of any noticeable probe vibrations, these pressure fluctuations point to slight shock oscillations, induced by the interference of the oblique shock wave with the normal probe shock.

The interference effects (2) are smallest for the pitot probe and biggest for the static pressure probe. Apparently, the shock boundary layer interference effects on the cone probe are stronger than any other interference effects. Since all three measured pressure values (P_{pit}, P_{cone}, ΔP_{LR}) are required to evaluate the actual flow conditions, these are necessarily in error within the region which is dominated by the pressure rise.

Moving the probe at a certain speed makes matters worse. Due to the damping effect of the pressure connecting tubes the response of the probe to a sudden pressure variation is too slow and the recorded pressures start to lag behind the corresponding stabilized pressure values. This time lag increases rapidly with increasing probe speed. However, the effect is not the same for all three pressures. Due to smaller sensing holes the static pressure is affected most. At a probe speed of 0.8 mm/s the overall pressure rise length increases from 2.0 mm (stabilized pressure) to 2.8 mm, but more importantly, the local pressure difference with respect to the stabilized pressure values reaches up to 50% of the overall static pressure rise.

The total pressure curve at 0.4 mm/s traversing speed shows an unexpected discontinuity in the pressure rise, which takes the form of a small plateau at about 40% of the overall pressure rise. Similar distributions were obtained at the same traversing speed with different types of pitot tubes (0.8, 1.5 and 2.0 mm diameters). This local plateau disappeared with increasing probe speed due to the long probe response time. On the other hand, this plateau pressure was not detected when measuring the stabilized pressure in fixed points because of a too large spacing between these points.

Effect of static pressure hole diameter : The effect of the hole size on the static pressure response time is demonstrated in Fig. 8. Compared to probe A with static pressure sensing holes of 0.4 mm Ø, probe B has holes of 3 mm diameter only, which allows to

reduce the distance between probe nose and pressure holes from 2.5 mm (probe A) to 1.5 mm, Fig. 3. The pressure rise lengths $\Delta\ell$ for both probe heads are given below :

Probe	A	B	A	B
Speed [mm/s]	0.4	0.43	0.8	0.85
$\Delta\ell$ [mm]	2.0	3.2	2.8	4.0

The maximum pressure difference between the two speed curves reached 25% of the overall pressure rise for probe A and 30% for probe B.

Effect of the length of connecting tubes : The effect of the length of the pressure connecting tubes on the static pressure rise at a traversing speed of 0.35 mm/s is presented in Fig. 9. An increase of the plastic connecting tube length by 1000mm increases the apparent pressure rise length from 1.7 mm (short connecting tubes) to 3.5 mm and the pressure lags behind by as much as 50% of the overall pressure rise.

4.2 Measurement error

The different pressure rise time for the three pressure sensors and the strong effect of hole size, traversing speed and pressure tube connection length on the pressure response time must lead to non-negligable errors when these pressure data are combined to evaluate the true local total and static pressures and flow angle.

In high speed cascade measurements the pressure data are used to calculate the blade performance in terms of total pressure loss coefficient or, and this is mostly the case for turbine cascades, in terms of the kinetic energy loss coefficient :

$$\zeta = 1 - \frac{1 - \left[\frac{P_{s_2}}{P_{o_2}}\right]^{\frac{k}{k-1}}}{1 - \left[\frac{P_{s_2}}{P_{o_1}}\right]^{\frac{k}{k-1}}}$$

where the indices 1 and 2 refer to the upstream and downstream measurement plane, respectively. Applied to the present experiment, P_{o_2} and P_{s_2} are the total and static pressure values in the traverse plane at the nozzle exit and P_{o_1} is the total pressure measured in the subsonic part of the convergent-divergent nozzle. P_{o_2} and P_{s_2} were evaluated using the measured values P_{pit}, P_{cone} and ΔP_{LR} and the probe calibration curves obtained previously in a uniform flow environment. As long as the probe heads are upstream of the shock, ζ must be obviously zero. Downstream of the shock, the probe records the shock losses. However, in the present case the oblique shock losses are very small, the kinetic energy losses amount to ζ=0.1% only (total pressure ratio across the shock P_{o_2}/P_{o_1}=0.9988).

Figure 10 shows for probe B the distribution of measured local losses ζ and Mach numbers M at different traversing speeds. Except for the shock losses of ζ=0.1%, any other deviation of ζ from zero presents a measuring error. The type of measurements errors we are faced with here are (see introduction) :

(1) basic errors covering all errors incurred in low gradient flow fields (non-linearity of instrumentation, calibration errors, fluctuations of overall flow conditions, etc);
(2) pressure gradient errors related to existence of strong pressure gradients in the flow field.

Upstream of the shock, ζ varies in an irregular fashion between +0.5% and -0.3% without any particular tendency as regards the traversing speed. These deviations of ζ from zero present

measurement errors of type (1), for which an error band of ± 0.3% seems to be realistic. As soon as the probe starts to "see" the shocks, ζ increases rapidly and reaches maximum local values of -1.3% at zero speed (i.e. measurements after pressures have stabilized in each measuring point), -2% at 0.43 mm/s probe speed and 2.9% at 0.85 mm/s. These maximum values are recorded in the early stage of the Mach member drop (i.e. static pressure rise) through the shock. The subsequent decay of ζ occurs at a much lower rate. All ζ values exceeding the basic error band of ± 0.3% are pressure gradient errors and depend strongly on the probe speed. Since in the present case, the pressure gradient error is caused by an overestimation of the pitot probe bow wave losses due to a too low static pressure reading - the recorded pressure lags behind the true static pressure - it turns out that P_{o_2}

$$P_{o_2} = P_{pit} + \Delta P_{o\ \text{bow wave}}$$

is bigger than P_{o_1} and ζ becomes negative.

It is somehow embarassing to state that the pressure gradient error is direction dependent. Indeed, if the probe would have traversed the shock coming from the high pressure side, the probe static pressure reading would have been too high within the shock region, resulting in too low a Mach number and consequently in too low wave losses and therewith positive ζ-values.

5. THE PRESSURE GRADIENT TEST : A STANDARD PROCEDURE FOR PROBE TESTING AND MEASUREMENT ERROR EVALUATION

In view of the significance of this relative easy experiment it is proposed to adopt the pressure gradient test as acceptance test for the use of pressure probes in transonic and supersonic cascade testing. It will help designing appropriate probes and selecting the correct combination of probe traverse speed and pressure tube length. Furthermore it offers a practical solution to the problem of evaluating the measurement accuracy. Since a pressure gradient test as described before, implies, at the beginning and end of the traverse, measurements in uniform flow with different Mach numbers and flow angles, it allows to distinguish between the basic errors which are always present, whatever the flow field is like, and typical pressure gradient errors. A quotation of the error band in the low gradient flow outside the shock region and of the maximum local error inside this region for both traverse directions are more instructive than any error analysis.

No doubt, if the proposed pressure gradient test finds wide application, the confidence in supersonic blade performance data will be greatly enhanced. However, it must be clear that in what concerns straight cascade testing, important problems subsist, in particular the problem of non-periodic flow conditions.

6. CONCLUSION

A combined total-static-directional pressure probe was tested in a known pressure gradient field set up by a shock genator at the exit of a supersonic nozzle. The best aimed at determining the effect of probe speed, static pressure probe geometrie and connecting tube length on the probe response.

It is demonstrated that this simple pressure gradient test is an extremely useful and efficient way to evaluate the measurement error of pressure probes intended for supersonic cascade performance measurements. It is suggested that publications of supersonic cascade performance data should be complemented by information on the measurement error derived from a supersonic pressure gradient test.

7. REFERENCES

1. SIEVERDING, C.H.: Pressure probe measurements in cascades. In Modern Methods of Testing Rotating Components of Turbomachines,
AGARDograph 207, 1975.

2. SIEVERDING, C.H.: Calibration characteristics of a 16° cone probe,
Proc. Symp. on Measuring Techniques in Transonic and Supersonic Cascade Flow. At CERL March 1979,
CERL Report RD/2/N 166/79

FIGURES

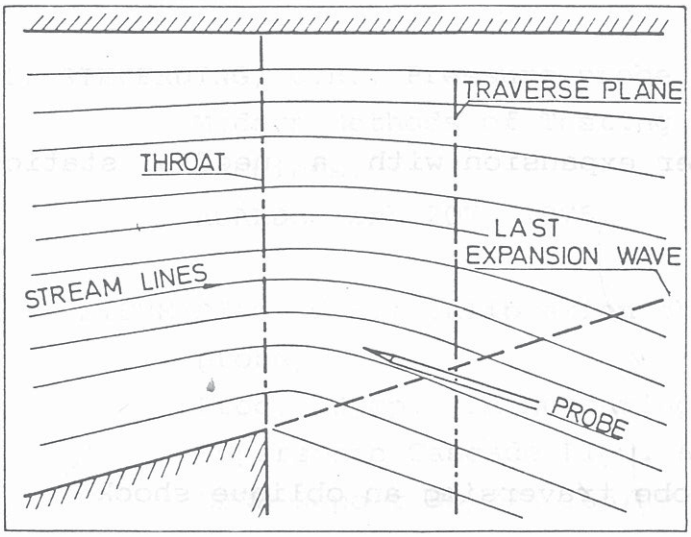
TRAVERSE PLANE
THROAT
LAST
EXPANSION WAVE
STREAM LINES
PROBE

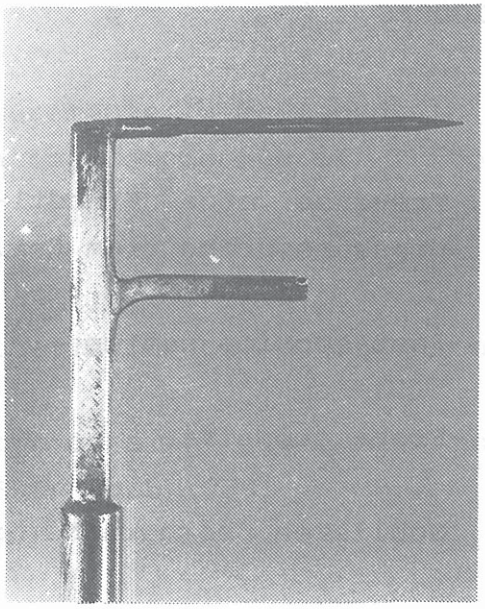

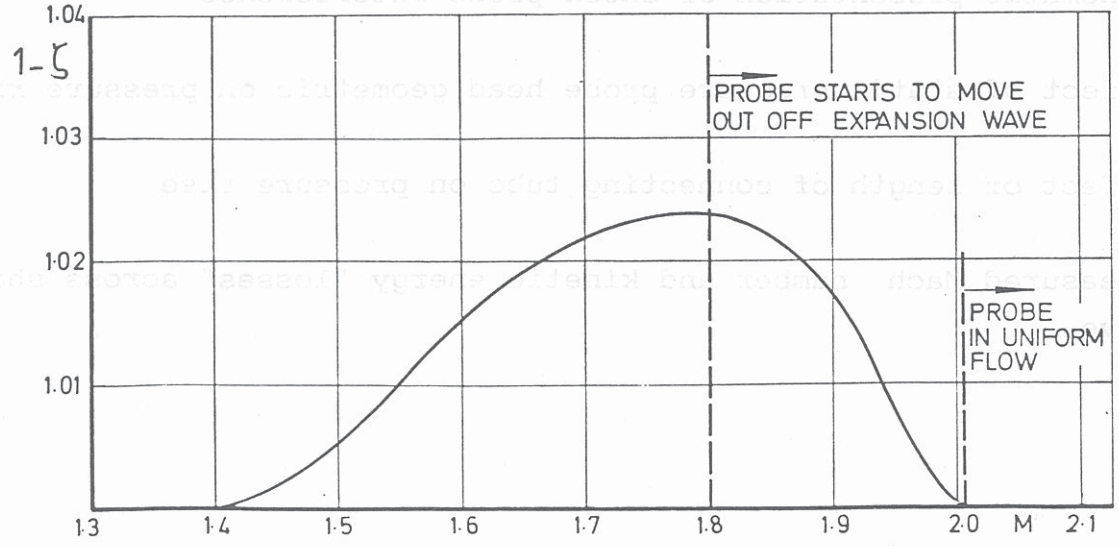
1-ζ
1·04
1·03
1·02
1·01
PROBE STARTS TO MOVE
OUT OFF EXPANSION WAVE
PROBE
IN UNIFORM
FLOW
1·3
1·4
1·5
1·6
1·7
1·8
1·9
2·0
M
2·1

Fig. 1

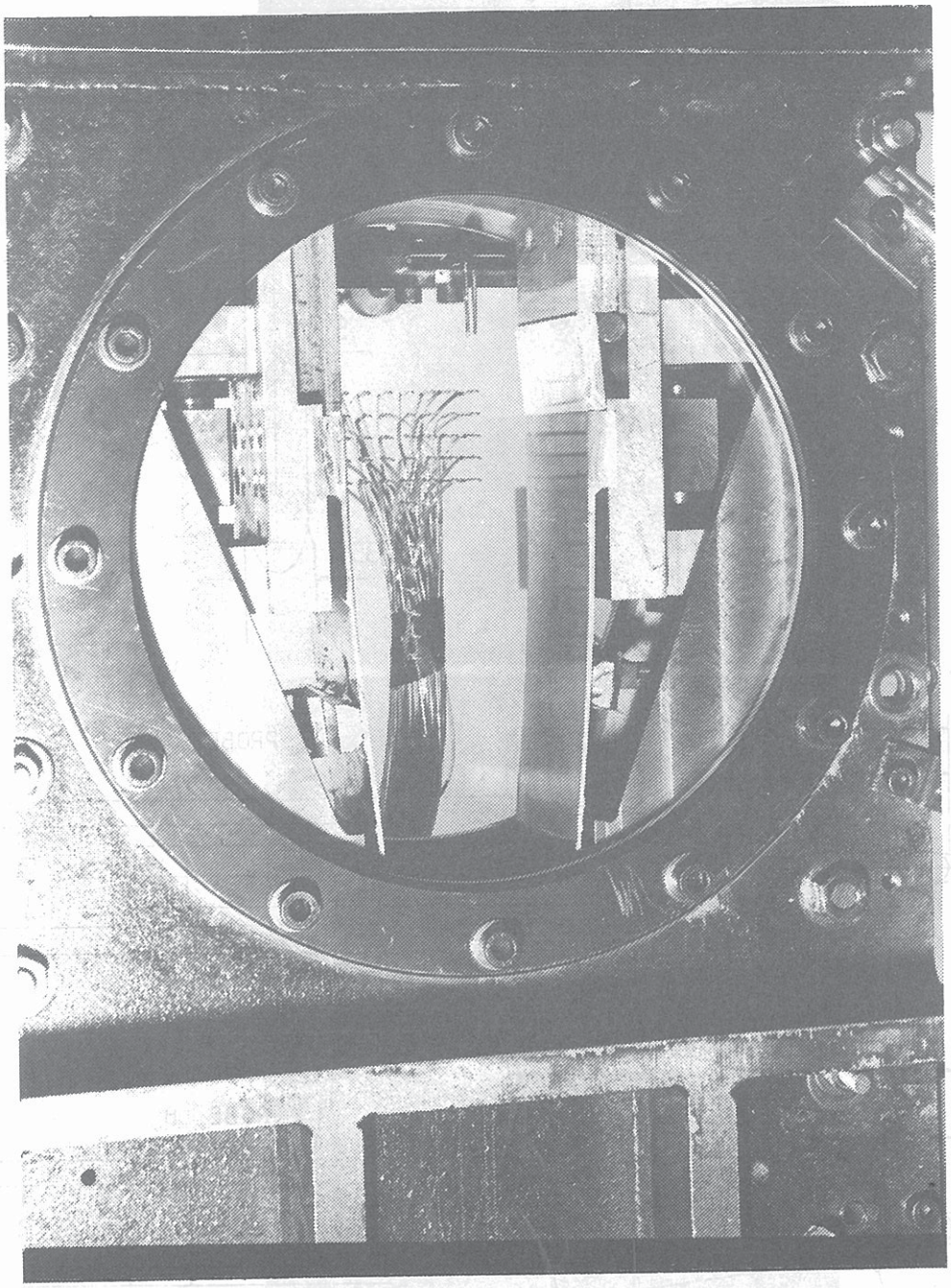

Fig. 2

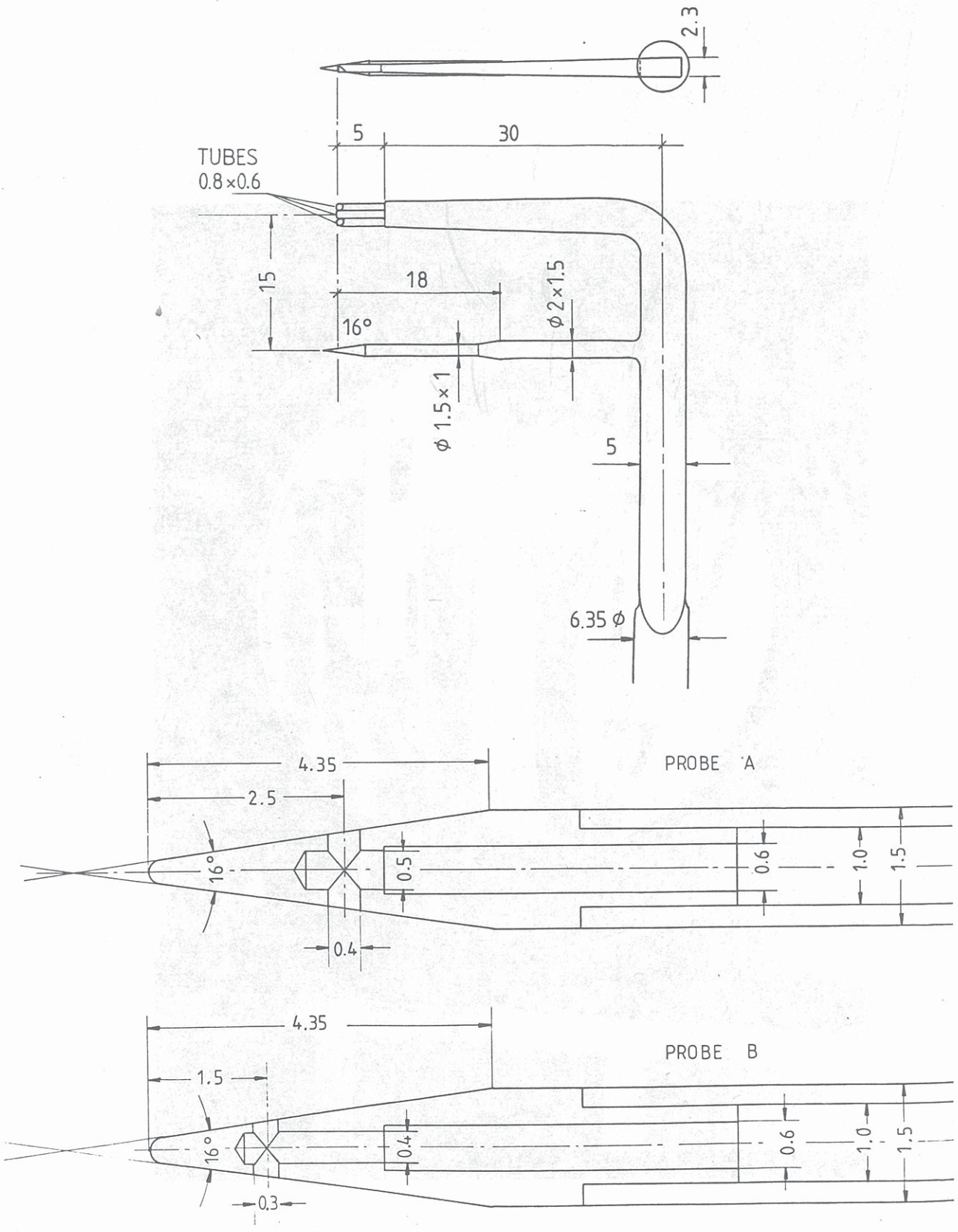

PROBE HEADS FOR STATIC PRESSURE PROBE

Fig. 3

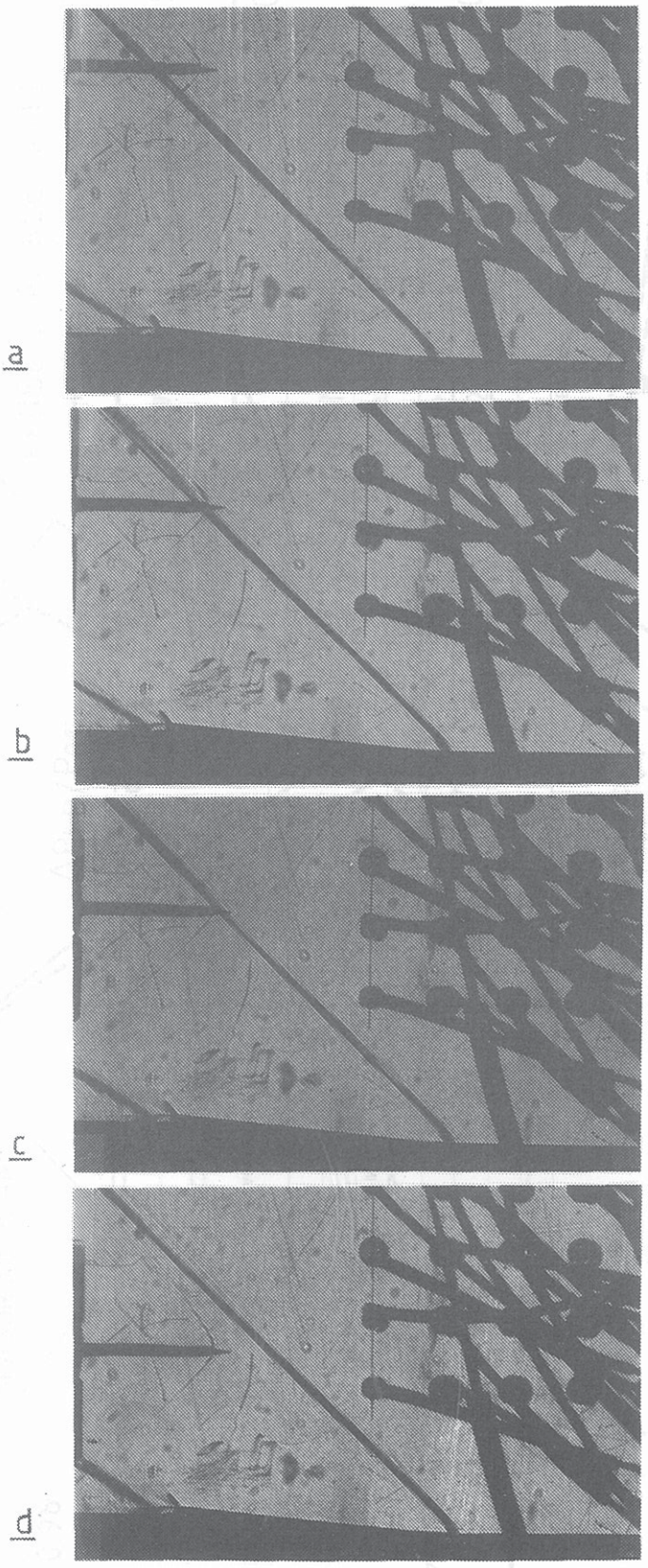

Fig. 4

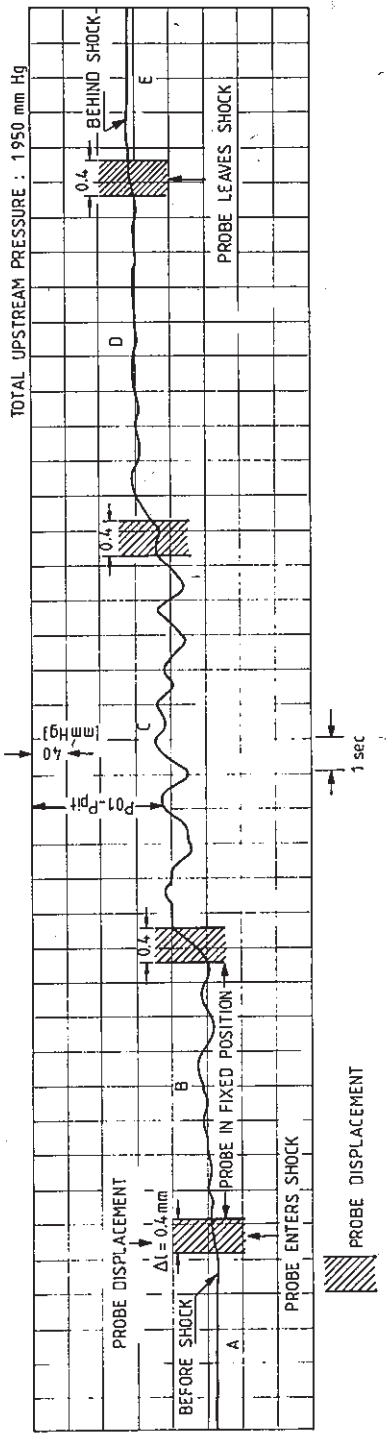
TOTAL UPSTREAM PRESSURE : 1950 mm Hg
BEHIND SHOCK
PROBE LEAVES SHOCK
PROBE DISPLACEMENT
PROBE IN FIXED POSITION
PROBE ENTERS SHOCK
BEFORE SHOCK
Δl = 0.4mm
0.4
A
B
C
D
E
1 sec
PROBE DISPLACEMENT

Fig. 5

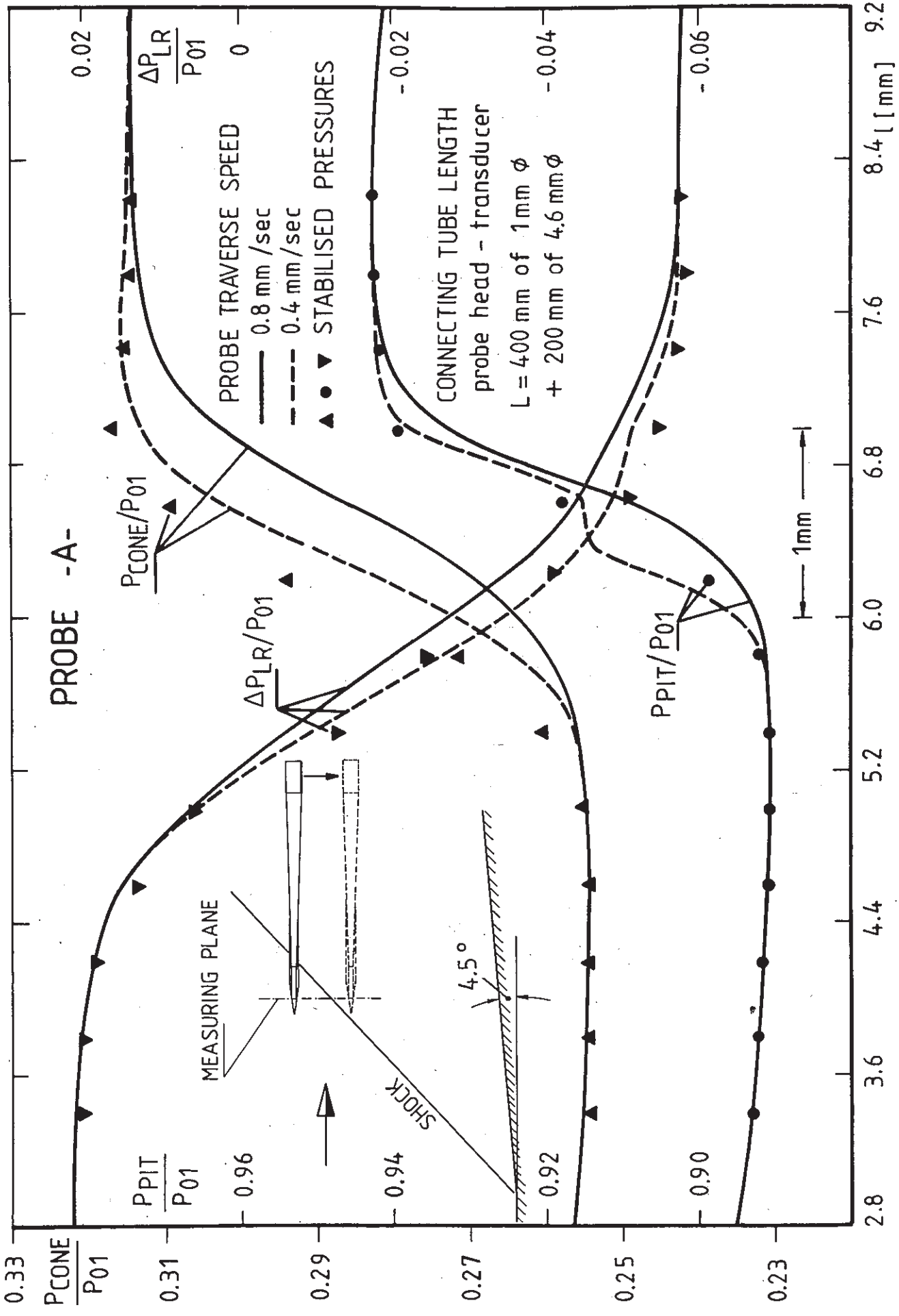
PROBE -A-
PROBE TRAVERSE SPEED
0.8 mm /sec
0.4 mm /sec
STABILISED PRESSURES
CONNECTING TUBE LENGTH
probe head - transducer
L = 400 mm of 1mm ϕ
+ 200 mm of 4.6 mmϕ
MEASURING PLANE
SHOCK
4.5°
1mm
PCONE/P01
ΔPLR/P01
PPIT/P01
ΔPLR/P01
PCONE/P01
PPIT/P01
[mm]

Fig. 6

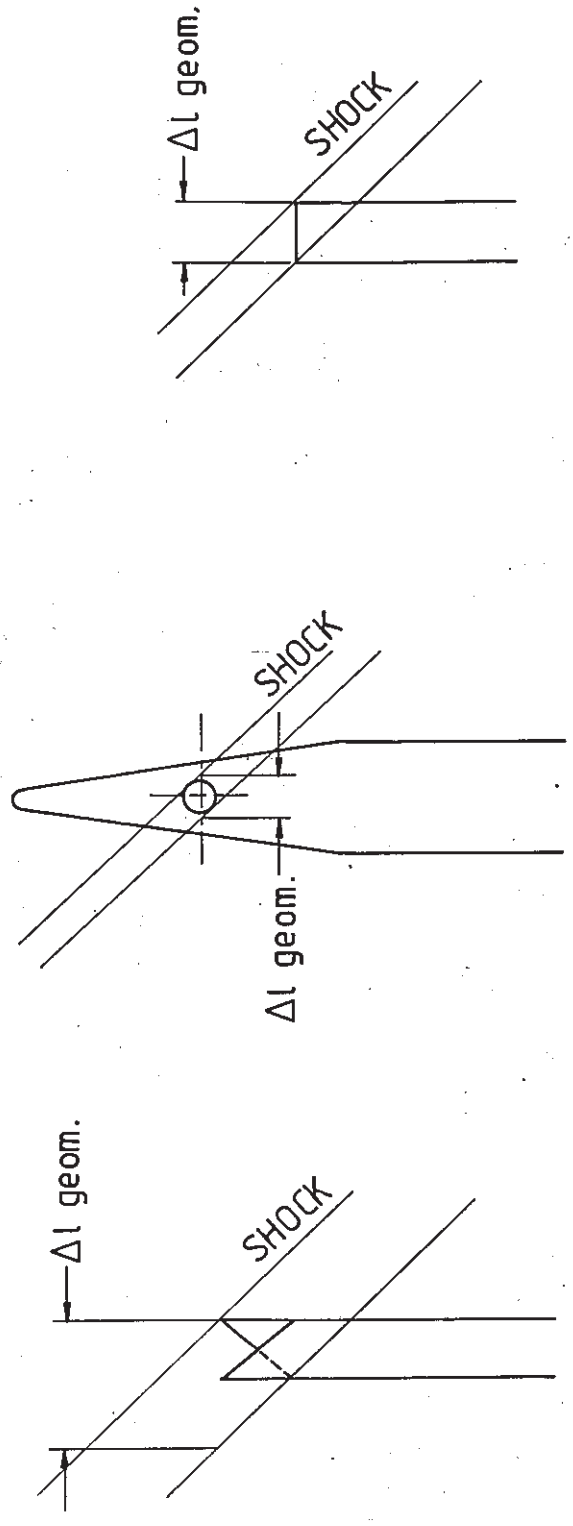

Fig. 7

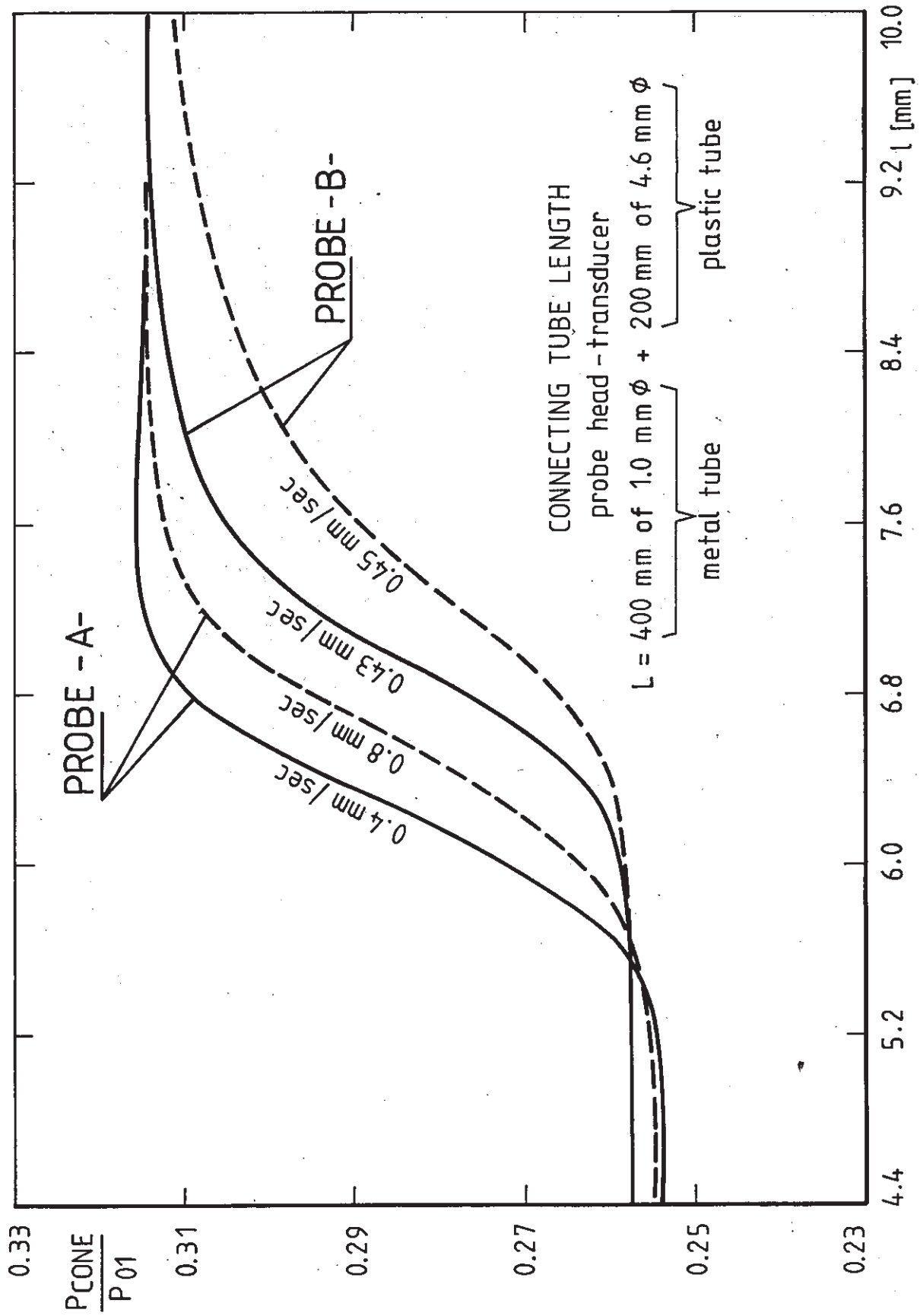
PROBE - A-
PROBE - B-
0.4 mm/sec
0.8 mm/sec
0.43 mm/sec
0.45 mm/sec
CONNECTING TUBE LENGTH
probe head - transducer
L = 400 mm of 1.0 mm ϕ + 200 mm of 4.6 mm ϕ
metal tube
plastic tube
PCONE / P01
0.33
0.31
0.29
0.27
0.25
0.23
4.4
5.2
6.0
6.8
7.6
8.4
9.2
10.0
l [mm]

Fig. 8

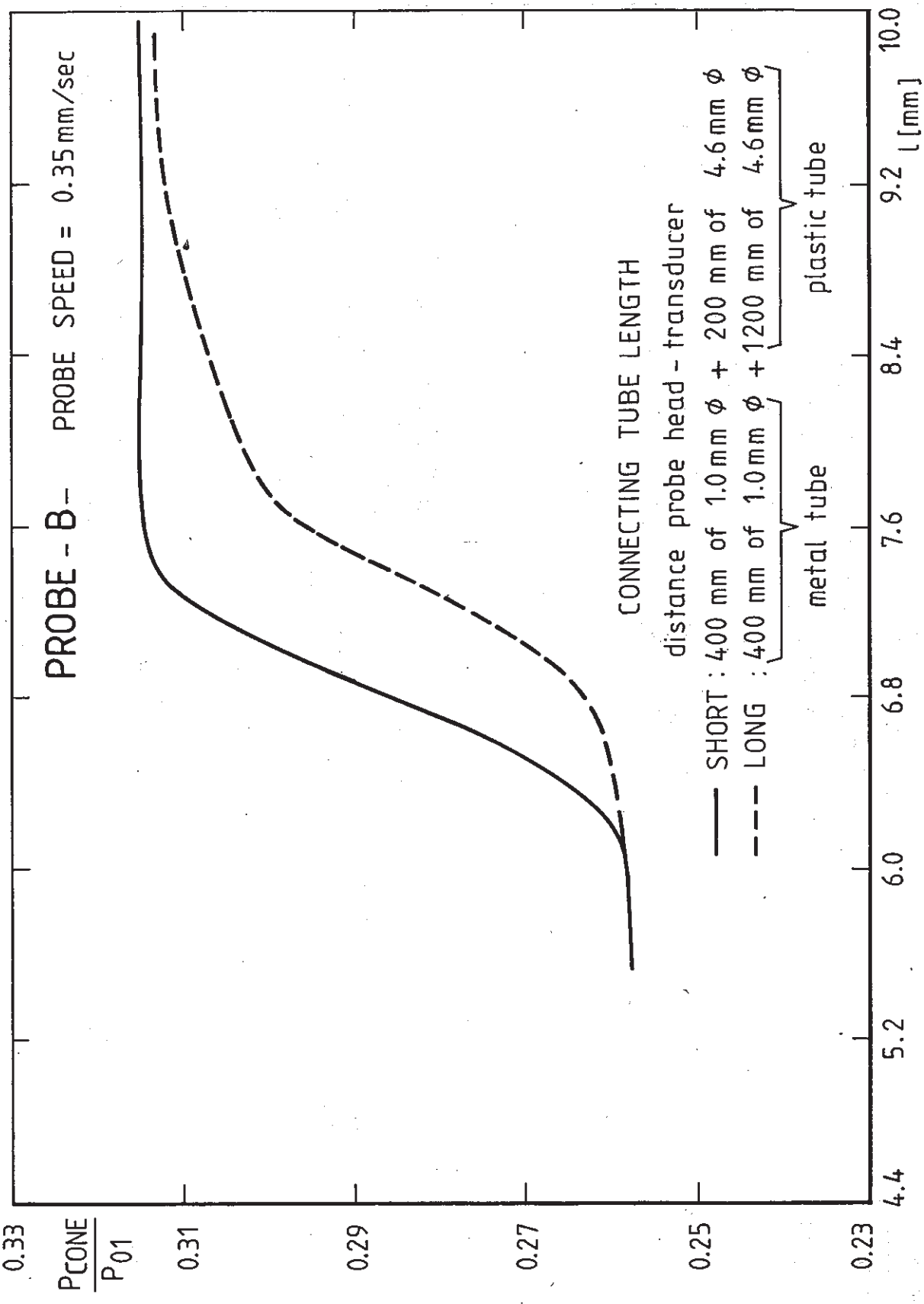
PROBE - B -
PROBE SPEED = 0.35 mm/sec
$\frac{P_{CONE}}{P_{01}}$
0.33
0.31
0.29
0.27
0.25
0.23
4.4
5.2
6.0
6.8
7.6
8.4
9.2
10.0
l [mm]
CONNECTING TUBE LENGTH
distance probe head - transducer
SHORT : 400 mm of 1.0 mm ϕ + 200 mm of 4.6 mm ϕ
LONG : 400 mm of 1.0 mm ϕ + 1200 mm of 4.6 mm ϕ
metal tube
plastic tube

Fig. 9

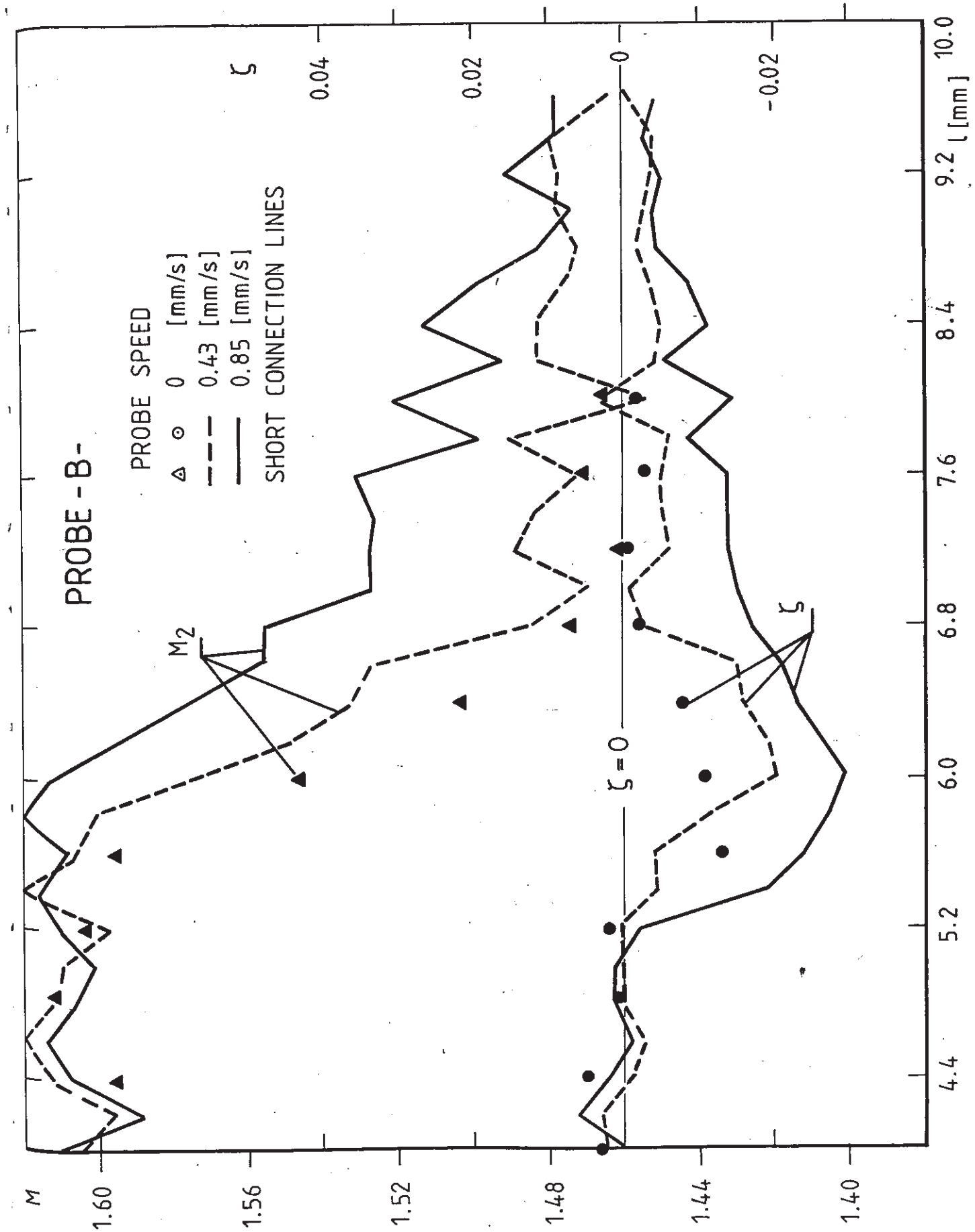
PROBE - B -
PROBE SPEED
Δ ○ 0 [mm/s]
0.43 [mm/s]
0.85 [mm/s]
SHORT CONNECTION LINES
M
ζ
M2
ζ = 0
1.60
1.56
1.52
1.48
1.44
1.40
0.04
0.02
0
-0.02
4.4
5.2
6.0
6.8
7.6
8.4
9.2
10.0
l [mm]

Fig. 10